**Proceedings of the 17th World Congress**
**The International Federation of Automatic Control**
**Seoul, Korea, July 6-11, 2008**

# Reliable Model and Cluster Aided Formation of Parametric Images in Functional Imaging

**Lingfeng Wen*,**,***, Stefan Eberl***,*, David Feng*,***

** Biomedical & Multimedia Information Technology (BMIT) Group, School of Information Technologies, J12, University of Sydney, NSW 2006, Australia*
*** Center for Multimedia Digital Signal Processing, Dept. of Electronic & Information Engineering, Hong Kong Polytechnic University, Hung Hom, Kowloon, Hong Kong*
**** Department of PET & Nuclear Medicine, Royal Prince Alfred Hospital, Missenden Road, Camperdown, NSW 2050, Australia*

**Abstract:** Parameter estimation in functional imaging provides unique quantitative measures in clinical diagnosis, and in the evaluation of treatment response and new drugs. Voxel-by-voxel parameter estimations can construct parametric images which visualize the spatial distribution of functional parameters. The low signal-to-noise ratio in single photon emission computed tomography (SPECT) may cause physiologically meaningless estimates using the general linear least square method (GLLS). A proof-of-principle framework is proposed in this study for constructing simultaneously multiple parametric images using a model-aided GLLS method and fuzzy clustering for dynamic SPECT. Computer simulations were performed to evaluate the accuracy and reliability of estimates for the studied methods. The results show that the model-aided GLLS with fuzzy clustering did enhance reliability for voxel-by-voxel parameter estimation with a slight overestimation of the volume of distribution. The method employing normalization of TTAC was superior to the method without normalization.

## 1. INTRODUCTION

Kinetic modeling in functional imaging has been used to build suitable models for biological systems and describe *in-vivo* dynamic behavior in a concise manner. Rate constants and macro parameters derived from rate constants of kinetic models are directly related to functional processes, providing unique quantitative measures in clinical diagnosis, and in the evaluation of treatment response and of new drugs.

Parameter estimation is a process to derive estimates of rate constants with regard to known functions for a biological system. In functional imaging, the input function (IF) is usually a sampling curve representing tracer activity in plasma, while the output function is a tissue time activity curve (TTAC) for a region of interest (ROI) drawn on dynamic data. Parametric images derived by voxel-by-voxel parameter estimation depict the spatial distribution of functional parameters without the need for manual delineation of ROIs (Feng 2007).

The non-linear least square (NLS) method is a standard technique for parameter estimation with statistically optimal outcomes (Huang 1980). However, due to intensive computational cost and the requirement for "good" initial estimates, NLS is not suitable for constructing parametric image. Through suitable integrations, the non-linear kinetic model equations can be transformed into a linear algebraic estimation problem (Johnson 1992) and linear least squares (LLS) methods can then be used to estimate the parameters. However, overlapping integration of the noise leads to biased estimates with this approach. The general linear least square (GLLS) method has thus been proposed to address the problem of LLS and aimed to provide fast and unbiased parameter estimation (Feng 1996). GLLS has been successfully applied in the studies of the brain, heart and liver for positron emission tomography (PET) (Feng 1996; Chen 1998; Choi 2006).

Single photon emission computed tomography (SPECT) also provides functional images, but has lower signal-to-noise ratio (SNR) than PET. Although SPECT has the potential of providing quantitative information (Almeida 1999), low SNR in SPECT data may cause physiologically meaningless estimates using GLLS in voxel-by-voxel parameter estimation. Several approaches have been proposed to enhance reliability of GLLS when dealing with noisy SPECT data. One approach is to use a statistical resampling technique to generate a set of synthetic curves, with the final parameters estimates being derived from the mean of the parameters derived from the fits to the synthetic curves (Wen 2006). The major drawback of this technique is the computational cost due to more curves having to be fitted. Recently, a fast regressive approach of GLLS was proposed using a flexible modeling technique to facilitate fast formation of parametric images. Despite of improved reliability, this model-aided method did not achieve complete elimination of all physiological meaningless fits (Wen 2007).

Clustering analysis classifies data into groups according to their intrinsic similarity. Clustering analysis has been applied to improve SNR in the spatial domain of data for constructing parametric images (Kimura 1999; Wen 2007). "Hard" clustering, such as K-mean clustering, assigns instances to one

specific cluster. In contrast, fuzzy clustering allows each instance to be associated with every cluster to a certain degree, which is referred to as "soft" clustering. The benefit of fuzzy clustering is that each instance contributes to all the cluster centroids in terms of fuzzy membership, largely avoiding issues of misclassification and over-smoothing in "hard" clustering.

In this study, we propose a proof-of-principle framework for constructing simultaneous multiple parametric images using the model-aided GLLS method and fuzzy clustering. Monte Carlo simulations were used to simulate dynamic SPECT data with the kinetics of the nicotinic receptor tracer 5-[$^{123}$I]-iodo-A-85380. Quantitative analysis was performed to evaluate the proposed methods with and without normalization of TTACs.

## 2. METHODS

### *2.1 Model-aided GLLS*

In system identification, several potential kinetic models can be used in the search of the best model which describes a biological system. For example, three-compartment four-parameter kinetic model (Fig.1) was the best kinetic model for the nicotinic receptor study, while two-compartment two-parameter model (Fig.2) may provide approximate estimation of some parameters with higher reliability.

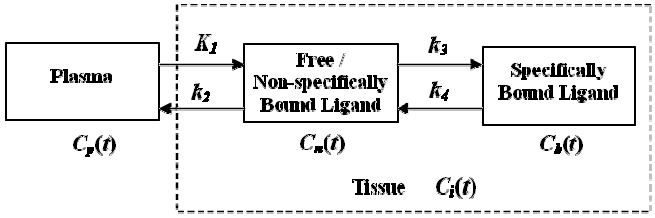


Fig.1. Three-compartment and four-parameter kinetic model for neuroreceptor studies. $C_p(t)$ is IF, $C_t$(t) is TTAC. $K_1$, $k_2$, $k_3$ and $k_4$ are the rate constants connecting adjacent compartments.

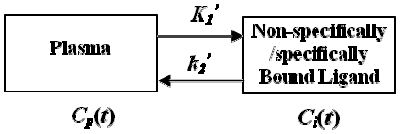


Fig.2. Two-compartment and two-parameter kinetic model. The definitions of the variables are the same as above ($V_d=K_1'/k_2'$).

Volume of distribution, $V_d$, is a relatively stable functional parameter, demonstrating the equilibrium distribution of tracer in the tissue. Equation (1) gives the definition of volume of distribution using rate constants for the three-compartment four-parameter model (Fig.1).

$$V_d = \frac{K_1}{k_2}\left(1+\frac{k_3}{k_4}\right) \tag{1}$$

Our previous investigation found that there was a linear relationship for $V_d$ between the two models (Figs. 1 and 2) . This implied that $V_d$ derived from the two compartment model could be used as a prior for parameter estimation from the 3 compartment model. The rate constants $k_3$ and $k_4$ are relatively sensitive to noise compared to $K_1$ and $k_2$, thus the model-aided GLLS assumed that estimates of $K_1$ and $k_2$ can be obtained using traditional GLLS (see Appendix for GLLS), while the prior $V_d$ can estimate $k_3$ using the slope of linear plots of $X$(t) vs. $Y$(t) according to equations (2) and (3),

$$X(t) = K_1(1+\beta)\int_0^t\int_0^t C_p(\tau)d\tau^2 - (1+\beta)\int_0^t C_t(\tau)d\tau - k_2\beta\int_0^t\int_0^t C_t(\tau)d\tau^2 \tag{2}$$

$$Y(t) = C_t(t) - K_1\int_0^t C_p(\tau)d\tau + k_2\int_0^t C_t(\tau)d\tau \tag{3}$$

where $\beta = K_1/(V_d k_2 - K_1)$ , followed by estimate of $k_4$ shown in (4).

$$k_4 = \beta \cdot k_3 \tag{4}$$

An optimization procedure was then applied to adjust $V_d$ regressively to minimize the residual sum of squares between measured $C_t(t)$ and estimated $C_e(t)$ (5).

$$J_{GLLS} = \arg\min_{V_d}\sum_{p=1}^{n}[C_e(t_p) - C_t(t_p)]^2 \tag{5}$$

$n$ is the number of dynamic frames. The initial $V_d$ was derived from $V_d$ for the two-compartment and two-parameter model (Fig.2).

### *2.2 Fuzzy Clustering*

A weighted least-square distance was used as a measure of closeness between the candidate voxel and centroid of cluster in the clustering (6).

$$D(C_j, R_k) = \sum_{i=1}^{n} w_i[C_j(t_i) - R_k(t_i)]^2 \tag{6}$$

$C_j$ is the TTAC of voxel $j$, $R_k$ is the centroid of cluster $k$. The weight function $w$ is proportional to the frame duration. A fuzzy C-means (FCM) algorithm was used in the data analysis with the objective function (7) (Pham 1999).

$$J_{FCM} = \arg\min\sum_{j\in\Omega}\sum_{k=1}^{M} u_{jk}^q D(C_j, R_k) \tag{7}$$

Here, $\Omega$ is the set of the voxels, $M$ is the total number of the clusters, $u_{jk}$ is the membership value at voxel location $j$ for cluster $k$ with $\sum_{k=1}^{M} u_{jk} = 1$, $q$ is a weighting exponent on each fuzzy membership.

FCM also employs an iterative process to achieve the objective function of (7) by updating fuzzy membership (8) and new centroid of each cluster (9), where $\Phi$ denotes the set of the clusters.

$$u_{jk} = \frac{1}{\sum_{s=1}^{M}\left[\frac{D(C_j, R_k)}{D(C_j, R_s)}\right]^{\frac{1}{q-1}}}, \forall j \in \Omega \quad (8)$$

$$R_k = \frac{\sum_{j\in\Omega} u_{jk}^q \cdot C_j(t)}{\sum_{j\in\Omega} u_{jk}^q}, \forall k \in \Phi \quad (9)$$

According to our prior investigation (Choi 2006; Wen 2007), total cluster number was set to 128 with $q$ = 1.1. Cluster centroids were initialized from randomly selected voxels. When the maximum change in the centroids over all clusters is less than a given value in an iteration, then convergence is deemed to have been reached.

*2.3 Proposed Methods*

Our currently proposed method (FM-GLLS) extends the recently developed model-aided GLLS with the aid of fuzzy C-mean clustering. Instead of parameter estimation for each voxel, the model-aided GLLS was used to fit the centroids of clusters. If any of the rate constants are negative or higher than 1 for a fit to a particular cluster centroid curve, then the memberships associated with that cluster are simply set to zero.

In constructing parametric images, parameter estimates from cluster $h$ then form the parameters for all the voxels which have their highest membership associated with cluster $h$ (10).

$$Voxel\{K_1, k_2, k_3, k_4\}_j = Cluster\{K_1, k_2, k_3, k_4\}_h$$
$$h = \arg\max(u_{jk}), j \in \Omega\, k \in \Phi \quad (10)$$

Here, $Voxel\{K_1, k_2, k_3, k_4\}_j$ denotes parameter estimates for individual voxel $j$, $Cluster\{K_1, k_2, k_3, k_4\}_h$ is the set of parameter estimates for the centroid of cluster $h$ by the model-aided GLLS.

We also investigated a second approach (FMN-GLLS), which incorporates normalization of TTAC and is based on FM-GLLS. The assumption of FMN-GLLS was that influx rate $K_1$ is a scale factor of the TTAC (Kimura 2002), whereas $k_2$, $k_3$ and $k_3$ describe the shape of TTAC. Voxel-by-voxel TTAC was normalized by its amplitude according to (11) before the clustering.

$$C_i^{norm}(t) = \frac{C_i(t)}{\int_0^T C_i(\tau)d\tau} \quad (11)$$

Here, $T$ is the total study duration. After the clustering and parameter estimation, equation (10) was then used in constructing parametric image except the estimate of $K_1$ was scaled as shown in equation (12).

$$K_1 = K_1^{norm} \cdot \int_0^T C_i(\tau)d\tau \quad (12)$$

*2.4 Computer Simulation and Parameter Evaluation*

High-count Monte Carlo simulations were performed to generate static projection data for individual brain structures based on a mathematical human brain phantom (Zubal 1994). The specifications of a Triad XLT triple head gamma camera (Trionix Research Laboratories, Twinsburg, OH, USA) were used in the simulation. Effects of attenuation, scatter, limited spatial and energy resolution, high-energy photon penetration of $^{123}$I were included in the simulations. The experimentally observed kinetics of the nicotinic receptor tracer 5-[$^{123}$I]-iodo-A-85380 (Kassiou 2001) was used to generate dynamic projection data according to a sampling schedule consisting of fifteen 1min scans, nine 5min scans and twelve 10min scans.

Five different levels of Poisson noise were added based on experimental observed noise levels and 20 sets of dynamic projection data were simulated at each noise level. The images were reconstructed by the OS-EM iterative method with 20 subsets and 2 iterations. Corrections were applied for attenuation, scatter and septal penetration of the high-energy photons of $^{123}$I.

GLLS, FM-GLLS and FMN-GLLS were used to generate parametric images. Influx rate $K_1$ and volume of distribution $V_d$ were chosen as the parameters of interest. Volumes of interests (VOI) derived from the mathematical phantom were used to generate the average parameters for the thalamus, cerebellum, and frontal cortex. Percentage bias and coefficient of variation (CV) of $K_1$ and $V_d$ were derived according to equations (13) and (14).

$$Bias = \frac{1}{MC}\left[\sum_{i=1}^{MC}\sum_{j=1}^{N}\frac{p_{i,j} - p_o}{N}\right] / p_o \times 100\% \quad (13)$$

$$CV = \frac{1}{p_0}\sqrt{\frac{\sum_{i=1}^{MC}(\sum_{j=1}^{N}\frac{p_{i,j}}{N})^2 - MC(\sum_{i=1}^{MC}\sum_{j=1}^{MC}\frac{p_{i,j}}{N})^2}{MC-1}} \quad (14)$$

Here, $MC$ is the total number of data sets, $N$ is number of voxels within a VOI, $p_o$ is the parameter reference value used to simulate the data.

## 3. RESULTS

*3.1 Percentage Bias*

Fig.3 shows the percentage bias for the frontal cortex at various noise levels. Despite similar bias (around -26%) achieved for the data without noise (noise level 0), GLLS substantially and increasingly underestimated $K_1$ with increasing noise levels. In contrast, stable estimates of $K_1$ were observed for the two investigated methods with -35.2±0.5% for FM-GLLS and -33.5±0.3% for FMN-GLLS.

High variation of bias of $V_d$ was obtained by GLLS with 17.1% for the moderate noise level and -29.5% for the highest noise level. Interestingly, FM-GLLS and FMN-GLLS

somehow compensated for the partial volume effect (PVE) and bias was slightly reduced for larger noise levels.

The higher bias of the estimates by GLLS was also evident in the thalamus. For a moderate noise level (noise level 3), the percentage bias of $K_1$ was -91.5% by GLLS, -31.6% and -14.4% by FM-GLLS and FMN-GLLS, respectively, while bias of $V_d$ was 53.8% by GLLS, -10.7% and -4.4% by FM-GLLS and FMN-GLLS.

Trends in the cerebellum were consistent with the findings in the thalamus and frontal cortex except for the overestimation of $V_d$ by FM-GLLS and FMN-GLLS as shown in Fig.4.

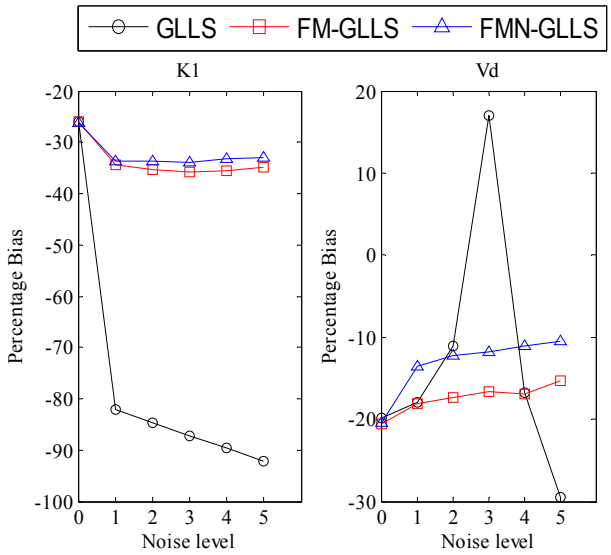


Fig.3 Plots of percentage bias for the frontal cortex as a function of increasing noise level (the number values of the abscissa denote simulated level of noise with 0 representing noise free)

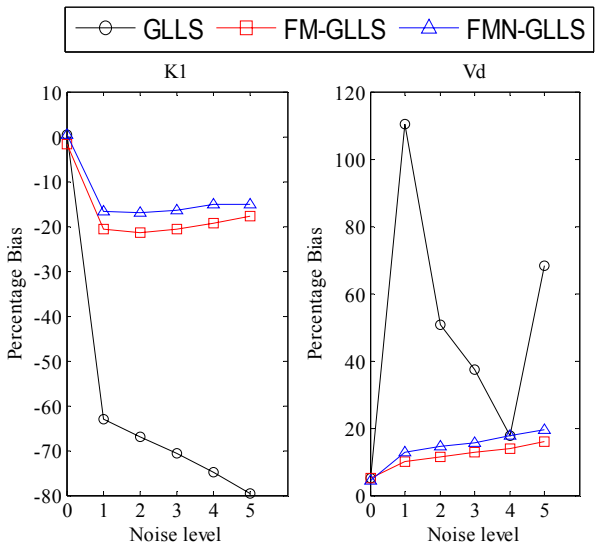


Fig.4 Plots of percentage bias for the cerebellum as a function of increasing noise level

In contrast to the estimates of $V_d$ for the noise-free data, higher $V_d$ was achieved for noisy data, e.g. $V_d$ by FMN-GLLS with an increased value of around 10% at the highest noise level for the three regions. This implies that the model-aided GLLS enhanced reliability for noisy voxel-wise TTACs at the expense of slight overestimation of $V_d$. For those regions suffering from PVE like thalamus and frontal cortex, the overestimation of $V_d$ to some extent compensates for PVE and provides more accurate estimates, but leads to over-estimation of $V_d$ in the cerebellum which is less affected by PVE.

### *3.2 CV*

CVs for the frontal cortex are plotted in Fig.5 as a function of noise level. High reliability was achieved for $K_1$ by all three methods with low values of CV (≤2.2%). However, extremely poor reliability of $V_d$ was also achieved by GLLS with values of CV exceeding 160%. This indicates that GLLS severely suffered from physiologically meaningless fits when dealing with voxel-wise parameter estimation. In contrast, high reliability of $V_d$ was achieved by FM-GLLS and FMN-GLLS (CV ≤2.9%).

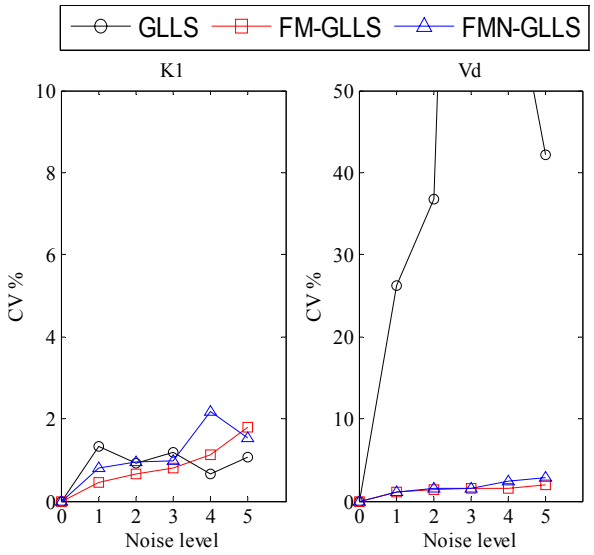


Fig.5 Plots of CV for the frontal cortex as a function of increasing noise level

Similar CV results were observed in the thalamus and cerebellum. The overall results of bias and CV demonstrated that the incorporation of FCM substantially improved the reliability of the model-aided GLLS. FMN-GLLS achieved more accurate estimates of $K_1$ and $V_d$ than FM-GLLS method due to normalization of TTAC, which allowed TTACs with similar shapes, but different scaling to be attributed to the same cluster, thus further improving the reliability of the estimates by reducing the dimensionality of the estimation.

### *3.3 Computational Cost*

Due to the required calculation of memberships associated with each cluster (128 clusters) for each voxel (around 90,000 voxels), the iterative updating of cluster centroids in FCM required substantial computational cost to achieve convergence. In this proof-of-principle evaluation of the proposed framework, the maximum number of iteration in FCM was limited to 20 for both FM-GLLS and FMN-GLLS. The total computation time of FM-GLLS and FMN-GLLS were about 6.5 and 5.0 times that of GLLS, respectively. Despite the similar run time, iteration number of FM-GLLS

reached 20 for all the data analyses, while FMN-GLLS required approximately 18 iterations. This demonstrates that the TTAC normalization step was efficient in reducing computational cost without affecting accuracy and reliability.

### *3.4 Parametric Image*

Fig. 6 shows the parametric images of $K_1$ and $V_d$ for the simulated data at the highest level of noise. There was a large number of 'black holes' in the parametric images by GLLS, showing physiologically meaningless fits. The two methods using FCM and model-aided GLLS clearly provided more reliable parametric images.

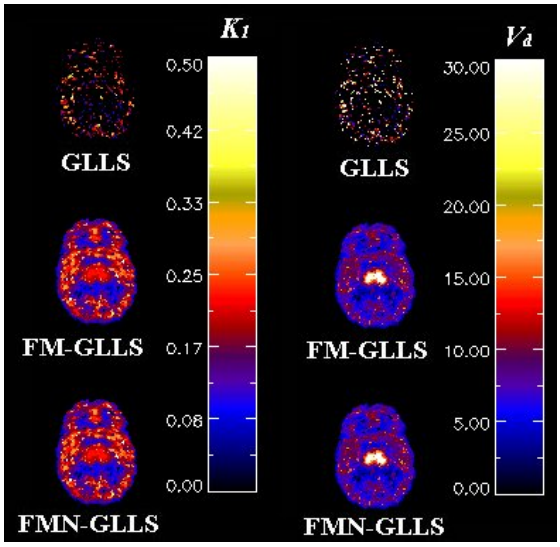


Fig.6 Parametric images of $K_1$ and $V_d$ for the highest noise level

Some outliers with higher value were also observed in the derived parametric images by FM-GLLS and FMN-GLLS. However, the fuzzy clustering technique largely improved SNR while conserving details of TTACs.

## 6. CONCLUSIONS

We propose a proof-of-principle framework for simultaneous formation of reliable multiple parametric images from noisy SPECT data. The proposed framework uses fuzzy c-mean clustering combined with a model-aided GLLS method. The simulation results demonstrate that the proposed methods achieve more accurate and reliable parametric images, but with a tendency to slightly overestimate $V_d$. Further investigations such as adaptive FCM clustering and optimal cluster number are warranted to maximize benefits of fuzzy clustering. The performance on clinical data will be investigated as well.

## ACKNOWLEDGEMENT

This work was supported in part by ARC, PolyU/UGC, and ISL/Australia-China special fund.

## REFERENCES

Almeida, P., M. J. Ribeiro, et al. (1999). Absolute Quantitation of Iodine-123 Epidepride Kinetics Using Single-Photon Emission Tomography: Comparison with Carbon-11 Epidepride and Positron Emission Tomography. *European Journal of Nuclear Medicine* **26**(12): 1580-1588.

Chen, K., M. Lawson, et al. (1998). Generalized Linear Least Squares Method for Fast Generation of Myocardial Blood Flow Parametric Images with N-13 Ammonia PET. *IEEE Transactions on Medical Imaging* **17**: 236-243.

Choi, H., L. Wen, et al. (2006). Fuzzy C-Mean clustering on kinetic parameter estimation with generalized linear least square algorithm in SPECT. *SPIE International Symposium on Medical Imaging*, San Diego, U.S, 1268-1277.

Choi, H.-C., S. Chen, et al. (2006). Fast Parametric Imaging Algorithm for Dual-Input Biomedical System Parameter Estimation. *Computer Methods and Programs in Biomedicine* **81**(1): 49-55.

Feng, D., S.-C. Huang, et al. (1996). An Unbiased Parametric Imaging Algorithm for Nonuniformly Sampled Biomedical System Parameter Estimation. *IEEE Transactions on Medical Imaging* **15**(4): 512-518.

Feng, D., L. Wen, et al. (2007). Techniques for Parametric Imaging. In: *Biomedical Information Technology*. D. Feng. San Diego, Elsevier press, 137-163.

Huang, S.-C., M. E. Phelps, et al. (1980). Noninvasive determination of local cerebral metabolic rate of glucose in man. *American Journal of Physiology* **238**: E69-E82.

Johnson, M. L. and L. M. Faunt (1992). Parameter-estimation by least-squares methods. *Methods in Enzymology* **210**: 1-37.

Kassiou, M., S. Eberl, et al. (2001). In vivo Imaging of Nicotinic Receptor Upregulation Following Chronic (-)-nicotine Treatment in Baboon Using SPECT. *Nuclear Medicine and Biology* **28**: 165-175.

Kimura, Y., H. Hsu, et al. (1999). Improved signal-to-noise ratio in parametric images by cluster analysis. *Neuroimage* **9**(5): 554-561.

Kimura, Y., M. Senda, et al. (2002). Fast formation of statistically reliable FDG parametric images based on clustering and principal components. *Physics in Medicine and Biology* **47**(3): 455-468.

Pham, D. L. and J. L. Prince (1999). Adaptive fuzzy segmentation of magnetic resonance images. *IEEE Transactions on Medical Imaging* **18**(9): 737-752.

Wen, L., S. Eberl, et al. (2007). Enhanced formation of parametric images using fast regressive GLLS for noisy functional imaging. *Proceeding of the 29th Annual International Conference of the IEEE*, Lyon, France, 4177-4180.

Wen, L., S. Eberl, et al. (2006). Enhanced parameter estimation with GLLS and the Bootstrap Monte Carlo method for dynamic SPECT. *Proceeding of the 28th Annual International Conference of the IEEE*, New York, U.S., 468-471.

Wen, L., S. Eberl, et al. (2007). Fast and Reliable Estimation of Multiple Parametric Images Using an Integrated Method for Dynamic SPECT. *IEEE Transactions on Medical Imaging* **26**(2): 179-189.

Zubal, I. G., C. R. Harrell, et al. (1994). Computerized 3-dimensional segmented human anatomy. **21**: 299-302.

## Appendix

For the three-compartment and four-parameter kinetic model (Fig.1), parameter estimation of GLLS can be given in (A1) for a given *N*-point TTAC.

$$\theta_{GLLS-3comp} = (Z^T Z)^{-1} Z^T r \tag{A1}$$

Here $\theta_{GLLS-3comp} = [P_1, P_2, P_3, P_4]^T$,

$$Z = \begin{bmatrix} \psi_1 \otimes C_p(t_1), \psi_2 \otimes C_p(t_1), \psi_1 \otimes C_i(t_1), \psi_2 \otimes C_i(t_1) \\ \psi_1 \otimes C_p(t_2), \psi_2 \otimes C_p(t_2), \psi_1 \otimes C_i(t_2), \psi_2 \otimes C_i(t_2) \\ \vdots \\ \psi_1 \otimes C_p(t_n), \psi_2 \otimes C_p(t_n), \psi_1 \otimes C_i(t_n), \psi_2 \otimes C_i(t_n) \end{bmatrix},$$

$$r = \begin{bmatrix} C_i(t_1) + \hat{P}_3 \psi_1 \otimes C_i(t_1) + \hat{P}_4 \psi_2 \otimes C_i(t_1) \\ C_i(t_2) + \hat{P}_3 \psi_1 \otimes C_i(t_2) + \hat{P}_4 \psi_2 \otimes C_i(t_2) \\ \vdots \\ C_i(t_n) + \hat{P}_3 \psi_1 \otimes C_i(t_n) + \hat{P}_4 \psi_2 \otimes C_i(t_n) \end{bmatrix}.$$

The values of $\hat{P}_3$ and $\hat{P}_4$ are denoted from the previous iteration of GLLS, followed by defining $\lambda_1$ and $\lambda_2$ in (A2).

$$\lambda_{1,2} = -(\hat{P}_3 \pm \sqrt{\hat{P}_3 + 4\hat{P}_4}) / 2 \tag{A2}$$

The values of $\psi_1$ and $\psi_2$ are given in (A3) and (A4).

$$\psi_1 = \frac{\lambda_2 e^{-\lambda_2 t} - \lambda_1 e^{-\lambda_1 t}}{\lambda_2 - \lambda_1} \tag{A3}$$

$$\psi_2 = \frac{e^{-\lambda_1 t} - e^{-\lambda_2 t}}{\lambda_2 - \lambda_1} \tag{A4}$$

Thus estimates of $K_1$ and $k_2$ are given in (A5) and (A6).

$$K_1 = P_1 \tag{A5}$$

$$k_2 = -(P_2 / P_1 + P_3) \tag{A6}$$